Chapter 12
Neuroscience

The brain is a remarkably complex organ; among other functions, it enables us to interpret sensation, produce actions, experience emotions, retain memories, and form decisions. Understanding how networks of brain cells compute and give rise to these functions is a central challenge in modern biology. Insights into neural computation have wide-reaching implications, from inspiring treatment of neurological disorders to understanding our sense of self. With recent advances in technology and infrastructure, we continue to increase our capacity to record signals from brain cells in much greater numbers and at ever-increasing temporal resolutions. Accordingly, the study of brain and neural systems is undergoing a phase change, from a science limited by our ability to acquire data to a science limited by our ability to understand complex data.

The brain is made up of an intricate, dynamic network of cells known as *neurons*. These neurons are tremendously heterogeneous in shape, function, and connectivity, and their organization has been the subject of systematic study since the 1880s, with the strikingly meticulous drawings of Santiago Ramón y Cajal, a few of which are reproduced in Figure 12.1. Neurons proliferate in number and connections during development, and these networks remain plastic throughout life; new cells and connections are continuously added to the network, and existing connections may be pruned and shaped by experience. To the best of our knowledge, the human brain contains 86×10^9 neurons and an approximately equal number of nonneuronal cells [11]. Each neuron makes on the order of 10^3 connections, or *synapses*, with other neurons. The network of connections between neurons, or more coarsely between brain areas, is known as the *connectome* [265].

12.1 ▪ Experimental techniques to measure neural activity

Neurons maintain and actively manage an electrical potential between the inside of the cell and the outside extracellular fluid across its cellular membrane. They encode and process information by a transient flux of ions across the cell membrane, a process mediated by a large family of proteins embedded within the cell membrane acting as gated ion channels. In most animal neurons, this ion flux culminates in an all-or-nothing electrical event known as an *action potential* or *spike*. The number and timing of these action potentials constitute the output of a neuron, through which one

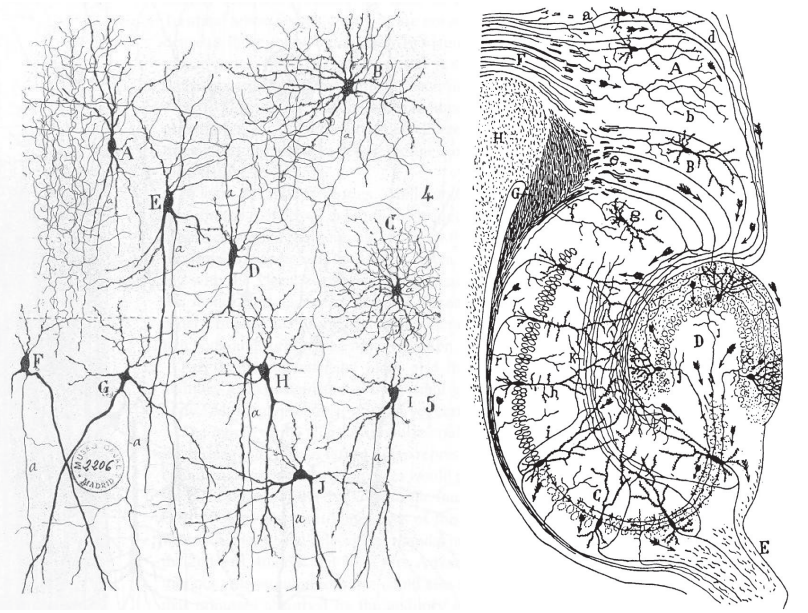

Figure 12.1. *Drawings of neurons by Ramón y Cajal. On the left are drawings of various types of neurons, sampling the diversity of shapes, sizes, and arborizations. On the right is a drawing of the neural circuitry of the hippocampus, a cashew-shaped brain structure associated with memory.*

neuron communicates with other neurons, muscles, or organs. Indeed, it is through monitoring this ion flux that we are able to observe neural activity and infer neural function.

The most detailed level of observation of electrical potentials requires mechanical attachment of a fine glass pipette onto a neuron. The voltage across the neuron's cell membrane is measured directly through filling the pipette with a conductive, biocompatible fluid. However, this class of intracellular or cell-attached recording is technically very challenging and prohibitively difficult to scale to more than a few neurons.

Extracellular experimental technologies to monitor neural activity can be electrical, optical, or magnetic in mechanism. The most direct form of observing neural activity is electrical. Because the flux of ions across the cell membrane induces a transient dipole, any conductive electrode within reasonable proximity of the neuron will act as an antenna and sense the dipole as a change in voltage. Electrodes vary in material, size, shape, and configuration. A fine wire electrode may be tens of micrometers in diameter, and when placed within a few micrometers of a neuron, it picks up changes in electrical potential from the neuron (as well as from any other active neurons in reasonable proximity). Signals from the same electrode, if filtered below approximately 300 Hz, are known as the *local field potential* of the region; these field potentials are thought to reflect some averaged activity of all the neurons within a diameter of hundreds of micrometers. Electrodes of large diameter placed under the skull and on top of the brain surface, in a technique known as electrocorticography (ECoG), acquire signals averaged from neurons over a larger radius still.

Optical methods of observing neural activity also monitor changes in voltage across the membrane, either directly with voltage-sensitive dyes or indirectly with fluorophores

detecting the influx of positively charged calcium ions across the cell membrane, known as *calcium imaging*. Imaging the brain has many advantages: it is possible to monitor many cells or brain areas simultaneously, and sometimes individual cells can be unambiguously resolved. The trade-offs are (i) that the temporal resolution of optical techniques tends to be orders of magnitude slower than using electrodes and (ii) it is difficult, but not impossible, to image brain areas at different optical depths.

These invasive techniques require surgical procedures to access the vertebrate brain (see, however, a remarkable exception in the case of imaging a larval zebrafish brain [5]). Even so, when invasive strategies are either infeasible or undesirable, noninvasive mechanisms to monitor neural dynamics include electrical recordings and magnetic imaging. Placing conductive electrodes on the surface of the skull, electroencephalography (EEG) records electrical signals from the brain, albeit heavily filtered through the intervening bone, cerebral spinal fluid, and dura mater. EEG is simple to perform and requires no surgery, but it suffers from poor spatial specificity and large measurement noise. Functional magnetic resonance imaging (fMRI) is similarly noninvasive; it measures spatially local changes in blood oxygenation levels through detection of differential response of the hemoglobin protein to a magnetic field when bound or unbound to oxygen. fMRI is performed using the same machine as used in clinical MRI, making it relatively accessible to neuroscientists. The tool is particularly appealing because of its ability to probe intact, normally functioning human brains, including peering into deep structure. However, its temporal resolution is low, sampling every 1 to 2 seconds, and the precise relationship between blood oxygenation levels and neural activity remains a subject of active research.

Despite the differences in measurement techniques, studying neural activity demands analysis of data that is high dimensional, complex, dynamic, and noisy. This chapter addresses the potential to analyze neural data using DMD.

12.2 ▪ Modal decomposition in neuroscience

Dimensionality reduction and dynamical systems theory have been powerful tools in understanding the measured activity of populations of neurons [74]. Despite the often staggering number of cells in a neuronal network, it has been observed that their activity often evolves on low-dimensional subspaces and can be described by relatively few distinct patterns [39, 311, 185, 67]. It follows that methods to discover these coherent patterns, especially unsupervised methods, play a pivotal role in understanding such complex data and enable formulation of new theories of mind.

12.2.1 ▪ Static methods

As in almost every other field of science and engineering, PCA is the most widely used modal decomposition algorithm to analyze neural data. Examples where PCA and PCA-derived techniques has been successfully applied to analyze high-dimensional neural recordings include experiments in insects [192, 232], fish [5], rodents [206, 69, 127], nonhuman primates [185, 67], and humans [62, 278], to name a few.

Beyond PCA, ICA is an alternative approach to dimensionality reduction that looks for components of the high-dimensional data space that are maximally independent from each other [22]. ICA is a technique commonly used in neuroscience to demix signals, for instance in fMRI data [55]. Another variant of static dimensionality reduction is nonnegative matrix factorization (NNMF), a method whose components are restrained to have nonnegative coefficients to allow interpretability [172].

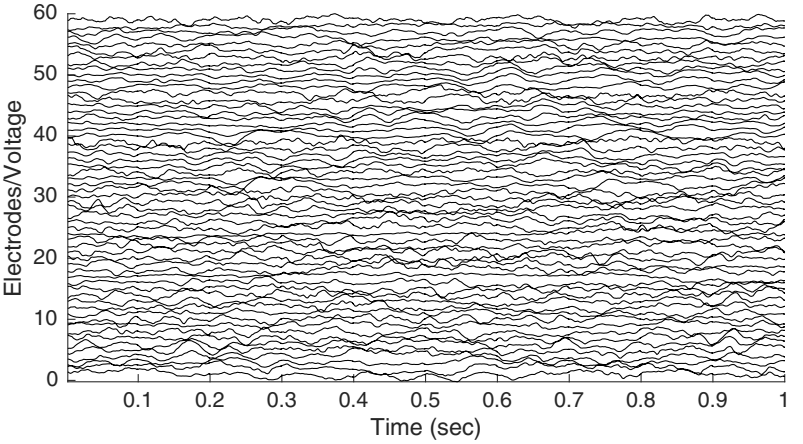

Figure 12.2. *An excerpt of a one-second window of ECoG recording from* 59 *electrodes. The normalized voltage trace as observed at each electrode is shown on the vertical axis, where electrode channels have been stacked with a vertical offset so they may be more easily visualized.*

12.2.2 ▪ Capturing dynamics

Time-series data has the additional feature that snapshots of data are acquired in sequence in time, and methods that leverage this temporal relationship are often able to capture low-dimensional structures hidden from purely static methods. One common strategy to denoise time-series data involves temporal smoothing, followed by application of PCA. This strategy leads to interpretation of high-dimensional time-series data as trajectories in lower-dimensional principal component space, where different experimental conditions may be compared and interpreted.

Another approach is to perform modal decomposition with an explicit dynamical model. These methods typically make some assumptions about the form of the dynamics and the noise, for instance, $\dot{x} = f(x) + \eta$, where $f(x)$ may be linear or nonlinear, and the noise η may be Gaussian or structured. Much progress has been made in advancing these models, as well as their interpretability in the context of neural recordings, and they include linear dynamical systems (LDS, [263]), Gaussian process factor analysis (GPFA, [311]), and nonlinear dynamical systems (NLDS, [310]). For a more comprehensive synthesis of methods broadly related to linear dimensionality reduction, see Cunningham and Ghahramani [73].

12.3 ▪ DMD on neural recordings

Here we show an example of DMD applied to neural recordings, expanding on ideas first described in Brunton et al. [44]. We start by analyzing a one-second window of neural activity recorded by a grid of electrodes placed at the human brain surface shown in Figure 12.2.[13] Here the voltage measured at each electrode is shown as a trace in time, where different electrode channels are offset so that they can be visualized. Recordings were subsampled at 500 samples/sec, high-pass filtered at 1 Hz, and normalized to have unit variance.

[13] The data used here is kindly shared by Jeffrey Ojemann.

In this example, and typically for many neural recordings one would like to analyze, the number of electrodes is exceeded by the number of snapshots in time. Following Chapter 7, our prescription for this scenario is to employ delay coordinates by stacking time-shifted copies of the recordings, thus augmenting the rank of the data matrix.

The following section of code loads this window of brain recording and computes its DMD.

ALGORITHM 12.1. **Demonstrate DMD on neural recordings (DMD_ECoG.m).**

```
load(['.' filesep 'Data' filesep 'ecog_window.mat']);

% parameters:
r = 200; % number of modes
nstacks = 17; % number of stacks

% construct the augmented, shift-stacked data matrices
Xaug = [];
for st = 1:nstacks,
    Xaug = [Xaug; X(:, st:end-nstacks+st)];%#ok<AGROW>
end;
X = Xaug(:, 1:end-1);
Y = Xaug(:, 2:end);

% SVD and truncate to first r modes
[U, S, V] = svd(X, 'econ');
U_r = U(:, 1:r);
S_r = S(1:r, 1:r);
V_r = V(:, 1:r);

% DMD modes
Atilde = U_r'*Y*V_r/S_r;
[W_r, D] = eig(Atilde);
Phi = Y*V_r/S_r*W_r;

% DMD eigenvalues
lambda = diag(D);
omega = log(lambda)/dt/2/pi;
```

12.3.1 ▪ The DMD spectrum

Let us start by examining the DMD eigenvalues λ. The visualization of these eigenvalues is shown in Figure 12.3. Note that since the raw data is strictly real valued, these eigenvalues are necessarily either real or come in conjugate pairs.

ALGORITHM 12.2. **Plot DMD eigenvalues of ECoG recordings (DMD_ECoG.m).**

```
figure('Position', [100 100 600 300]);
subplot(1,2,1);
plot(lambda, 'k.');
rectangle('Position', [-1 -1 2 2], 'Curvature', 1, ...
    'EdgeColor', 'k', 'LineStyle', '--');
```

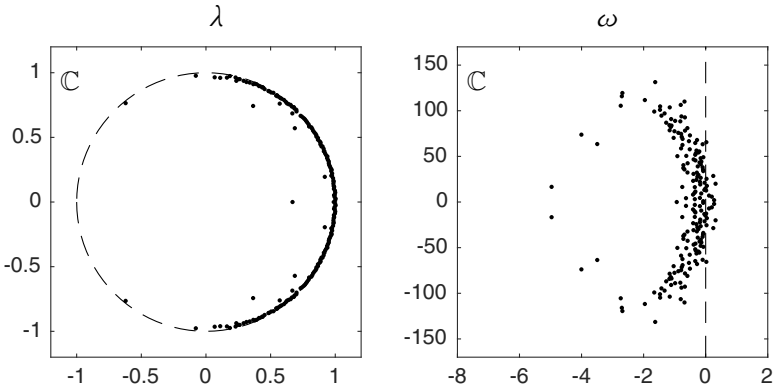

Figure 12.3. *DMD eigenvalues of the excerpt of ECoG recording shown in Figure* 12.2. *Here we are visualizing both the discrete time eigenvalues λ relative to the unit circle (dashed line on left panel) and the eigenvalues transformed to continuous time as $\omega = \log(\lambda)/(2\pi\Delta t)$ (right panel).*

```
axis(1.2*[-1 1 -1 1]);
axis square;


subplot(1,2,2);
plot(omega, 'k.');
line([0 0], 200*[-1 1], 'Color', 'k', 'LineStyle', '--');
axis([-8 2 -170 +170]);
axis square;
```

The magnitude of λ_i relative to the unit circle indicates the stability of the corresponding DMD spatial mode ϕ_i, where modes whose eigenvalues lie exactly on the unit circle are neutrally stable. The phase of λ_i indicates the oscillatory frequency of the mode. We make a change of units by taking the logarithm of λ and normalizing by Δt, $\omega = \log(\lambda)/(2\pi\Delta t)$, so that now the imaginary component of ω_i is the frequency of oscillation in units of cycles per second (Hz).

One way to make use of ω is to connect the frequencies of oscillation computed by DMD with the power spectrum of the data. This strategy of analyzing the DMD spectrum of the high-dimensional data leverages the extensive literature on frequency bands of brain oscillations, so that we may select spatial features based on well-defined frequency features such as beta and gamma band oscillations.

To visualize the DMD spectrum, we follow the scaling of each mode ϕ_i as described in Chapter 8 and plot these mode amplitudes against the imaginary component of ω_i.

***ALGORITHM* 12.3. Code to plot the DMD spectrum and compare to the power spectrum (DMD_ECoG.m).**

```
% alternate scaling of DMD modes
Ahat = (S_r^(-1/2)) * Atilde * (S_r^(1/2));
```

```
[What, D] = eig(Ahat);
W_r = S_r^(1/2) * What;
Phi = Y*V_r/S_r*W_r;

f = abs(imag(omega));
P = (diag(Phi'*Phi));

% DMD spectrum
figure('Position', [100 100 600 300]);
subplot(1,2,1);
stem(f, P, 'k');
xlim([0 150]);
axis square;

% power spectrum
timesteps = size(X, 2);
srate = 1/dt;
nelectrodes = 59;
NFFT = 2^nextpow2(timesteps);
f = srate/2*linspace(0, 1, NFFT/2+1);

subplot(1,2,2);
hold on;
for c = 1:nelectrodes,
    fftp(c,:) = fft(X(c,:), NFFT);
    plot(f, 2*abs(fftp(c,1:NFFT/2+1)), ...
        'Color', 0.6*[1 1 1]);
end;
plot(f, 2*abs(mean(fftp(c,1:NFFT/2+1), 1)), ...
    'k', 'LineWidth', 2);
xlim([0 150]);
ylim([0 400]);
axis square;
```

Figure 12.4 shows the DMD mode amplitudes and compares them to the Fourier transform of the same data. The two are qualitatively similar and have the same rough amplitude decay as frequency increases. To reiterate the key differences, DMD is computed as a decomposition of the full high-dimensional time-series data in this short-time window, whereas the Fourier transform is computed on each electrode's voltage trace separately. Moreover, the frequencies of DMD modes are not uniformly distributed, so that if regular sampling of frequency space is desired, some consolidation of modes may be necessary.

12.3.2 ▪ Interpretation of modes and dynamics

One key advantage of DMD as a means of analyzing neural recordings is its straightforward interpretation. DMD modes correspond to correlations in space at frequencies dictated by the DMD eigenvalues. To be explicit, we can unpack the representation of the high-dimensional time-series data above as illustrated in Figure 12.5. Mode magnitudes are visualized in electrode coordinates on the brain, along with their temporal evolution. Note that here we have not shown the phase component of the DMD modes, although these can likewise be interpreted as the relative phase between elec-

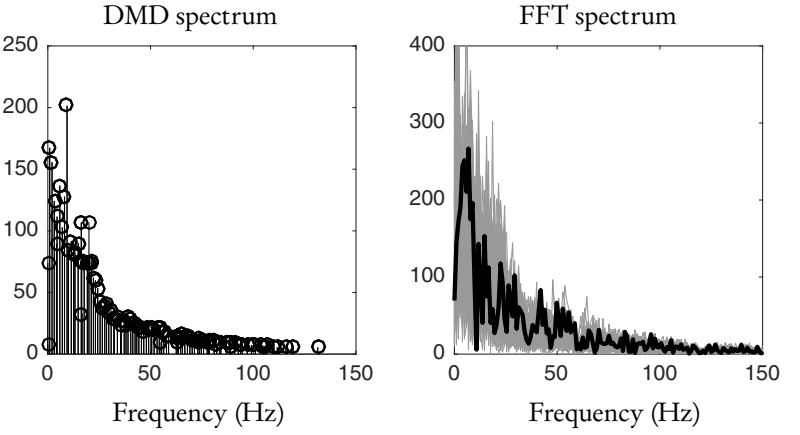

Figure 12.4. *The DMD spectrum qualitatively resembles the power spectrum as computed by FFT. Note that the FFT spectrum is computed separately for each electrode (gray lines), and their average is shown as the bold black line.*

trodes at each frequency.

The spatial patterns extracted as DMD modes with coherent dynamics at a particular frequency band are comparable, but not identical, to spatial patterns extracted by band-pass filtering each channel of recording at the same frequency band. One difference is that DMD eigenvalues are complex valued, so that the dynamics have growth/decay in addition to frequency of oscillation. This ability to capture growth/decay of spatial patterns is important when analyzing nonstationary signals and transient behaviors, especially in the context of mrDMD (see Chapter 5).

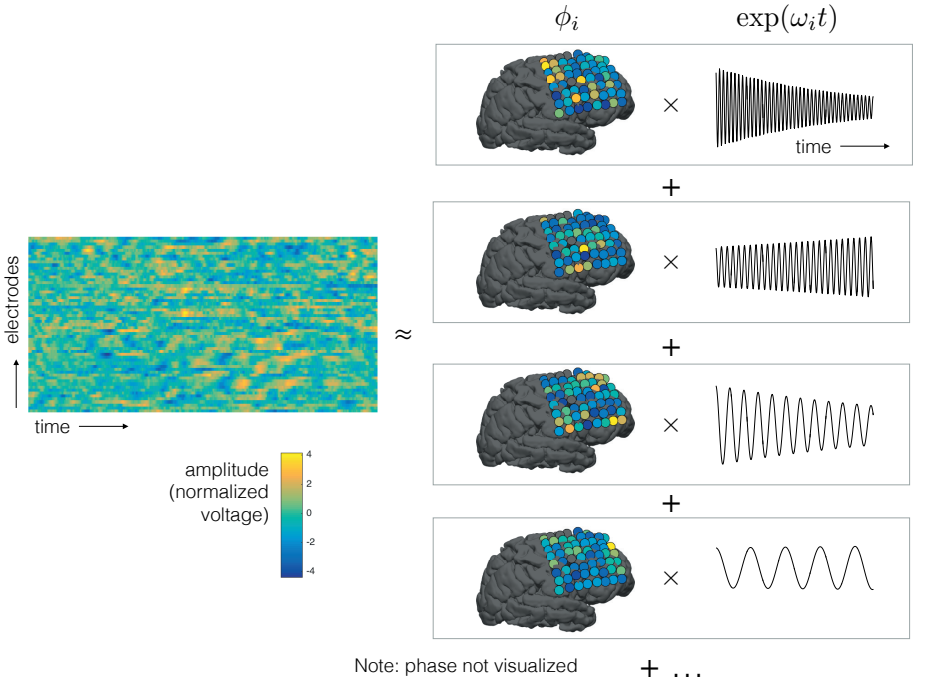

Figure 12.5. *An illustration of DMD modes interpreted in the context of ECoG recordings. The raw data, shown here as a heat map of voltage for every electrode over time, is decomposed into a sum of DMD modes, each of which has a spatial part and a temporal evolution part. The spatial modes can be readily interpreted as relative magnitudes of correlation among electrodes. These spatial modes also have phase components that are not visualized in this illustration, and these can be interpreted as relative synchrony between electrodes.*